

Metal-insulator transition in $\text{CaCu}_3\text{Fe}_4\text{O}_{12}$

Atsushi Hariki,^{1,2} Tatsuya Yamaguchi,¹ Mathias Winder,² and Jan Kuneš^{2,3}

¹*Department of Physics and Electronics, Graduate School of Engineering,
Osaka Prefecture University 1-1 Gakuen-cho, Nakaku, Sakai, Osaka 599-8531, Japan*

²*Institute of Solid State Physics, TU Wien, 1040 Vienna, Austria*

³*Department of Condensed Matter Physics, Faculty of Science,
Masaryk University, Kotlářská 2, 611 37 Brno, Czechia*

(Dated: May 6, 2024)

We study structurally-triggered metal-insulator transition in $\text{CaCu}_3\text{Fe}_4\text{O}_{12}$ by means of local density approximation (LDA) $+U$ and LDA+dynamical mean-field theory (DMFT). The ferrimagnetic insulating phase is essentially the same within both approaches. While LDA+ U describes the metal-insulator transition as a Peierls-like instability driven by Fermi surface nesting in the magnetically ordered phase, LDA+DMFT allows also the site-selective Mott transition without magnetic ordering as well as smooth crossover between the two pictures. We point out similarities and differences to rare-earth nickelates.

I. INTRODUCTION

Synergy of the charge, spin, orbital or lattice degrees of freedom is known to give rise to a plethora of different thermodynamic phases and transitions between them in transition-metal oxides (TMOs) [1, 2] with perovskite structure. Competition between crystal field, spin-orbit coupling and Hund's exchange leads to spin-state crossovers [3–5] and possibly to spin-state ordered phases [6, 7] or excitonic magnetism [8–10]. Different bonding between the TM e_g and t_{2g} orbitals with oxygen p orbitals leads to coexistence of local moments with itinerant electrons in some materials, e.g. doped manganites [11–13], while others are Mott insulators described by pseudospin models of Kugel-Khomskii type [2, 14]. The perovskite structure built out of corner-sharing oxygen octahedra allows various structural deformations. Rotations/tilting of the oxygen octahedra [15–17] affect the electronic bandwidths. Cooperative Jahn-Teller distortions [2, 18–20] strongly couple to orbital orders [21–24], while breathing distortions couple to charge order or site-selective Mott state [25–27].

In high-valence TMOs, which are metallic or close to metal-insulator transition (MIT), the charge degree of freedom adds to the complexity. Concomitant MIT and structural transition followed by unusual magnetic ordering attract much attention to rare-earth nickelates RNiO_3 [22, 25, 28–35]. Starting from the ionic picture, Mazin *et al.* [22] proposed the charge disproportionation (CD) $2d^7 \rightarrow d^6 + d^8$ to be the origin of a breathing distortion of NiO_6 octahedra and MIT. Park *et al.* [25] used LDA+DMFT and introduced the concept of the site-selective Mott transition. The CD was shown to emerge as an effective low-energy description of the site-selective Mott transition from LDA+DMFT calculations [36]. Lee *et al.* [28] took the band picture to argue that a Peierls-like distortion originating in Fermi surface nesting explains the physics of nickelates. This view is supported by LDA+ U calculations of Mercy *et al.* [34] in the magnetically ordered state who pointed out the importance of octahedral rotations for tuning the Peierls-

like instability. In this picture, the metal-insulator transition is connected with the magnetic ordering, which is at odds with the paramagnet-to-paramagnet MIT transition in a number of nickelates. The question of Peierls vs site-selective Mott mechanism [37] remains a subject of active debate. The site-selective Mott transition was reported also in Fe_2O_3 [26] under pressure.

In this Article, we study the iron oxide $\text{CaCu}_3\text{Fe}_4\text{O}_{12}$ (CCFO), which belongs to A-site ordered TM perovskites $\text{AA}'_3\text{B}_4\text{O}_{12}$ [38–43]. Iron in CCFO is proposed to have anomalously high Fe^{4+} valence [44]. In addition to common parameters in TMOs, such as intra-atomic Coulomb interaction, band filling or structural distortions, the interaction between TM ions on A' and B sites adds another control parameter in this group of materials.

The high-temperature crystal structure of CCFO belongs to $Im\bar{3}$ space group with a sizable rotation of FeO_6 octahedra, which can be viewed as a frozen M_2^+ mode (viewed as a rotation of the octahedra along the [111] axis) with a minor M_1^+ contribution (elongation of the octahedra along the [111] axis), see Figs. 1c,d and Supplementary Material (SM) [45]. The $M_2^+ + M_1^+$ distortion (with the experimental amplitudes) is referred to as the Q_R distortion hereafter. The Q_R distortion, which leads to a square-planar coordination of Cu with the four O neighbors (Fig. 1a), is common in the $\text{AA}'_3\text{B}_4\text{O}_{12}$ series. At 210 K, a structural phase transition to $Pn\bar{3}$ structure takes place simultaneously with MIT and magnetic transition. Although the Fe^{4+} ions may be expected to adopt the Jahn-Teller-active high-spin $t_{2g}^3 e_g^1$ configuration, a Jahn-Teller distortion has not been reported. Instead, a breathing distortion Q_B of the FeO_6 octahedra was observed in the insulating phase (Fig. 1b). This gives rise to two distinct Fe sites with short and long Fe–O bonds (Fig. 1a).

The concomitant electronic and structural deformation in CCFO is reminiscent of MIT in RNiO_3 (formally Ni^{3+} : $t_{2g}^6 e_g^1$) accompanied by the breathing distortion of NiO_6 octahedra. Parallel to the debate on RNiO_3 [22, 25, 29–35], it has been suggested that a CD of the type: $2(d^5 \underline{L}) \rightarrow d^5 \underline{L}^2 + d^5$ (\underline{L} : oxygen hole) takes

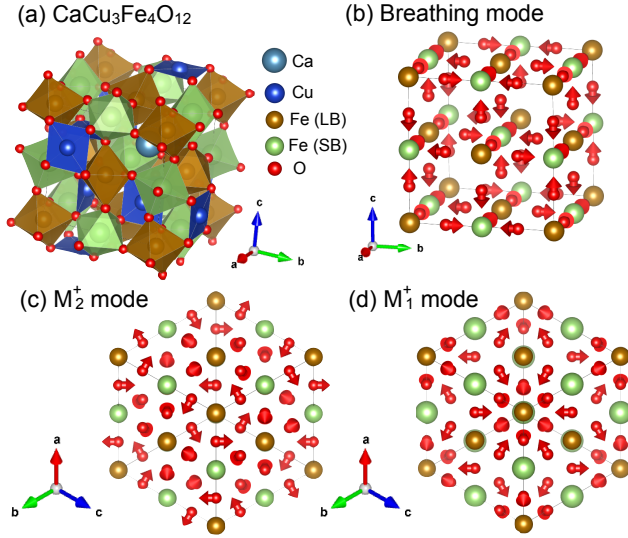


FIG. 1. (a) Low-temperature structure of $\text{CaCu}_3\text{Fe}_4\text{O}_{12}$ (space group $Pn\bar{3}$). (b) breathing distortion of oxygen atoms. (c) M_2^+ mode. (d) M_1^+ mode. The crystal structure is visualized using VESTA3 [49]. The mode analysis is performed using AMPLIMODE [50]. Cu (Ca) atoms sitting on $3/4$ ($1/4$) of the A sites in the ABO_3 perovskite lattice show no displacements from the high-symmetry positions in all temperatures. Thus, Cu and Ca atoms are not shown in panels (b)–(d).

place in the insulating phase of CCFO [42, 44, 46, 47]. It is worth pointing out that in nickelates the t_{2g} electrons form a spin singlet (t_{2g}^6), while in CCFO those tend to form a stable high-spin t_{2g}^3 state with $S = 3/2$ moment, and thus rather different magnetic behavior is to be expected. Indeed, along with at the MIT, a ferrimagnetic (FM) order with a large magnetization of $9.7 \mu_B/\text{f.u.}$ is observed [44, 48]. The large magnetization indicates a ferromagnetic alignment of the Fe moments antiferromagnetically coupled to the Cu^{2+} ($S = 1/2$) sublattice in CCFO.

We use the local-density approximation (LDA) + U and LDA + dynamical mean-field theory (DMFT) approaches to investigate the electronic response to the Q_R and Q_B distortion. We characterize the local state of Fe ions in the uniform and disproportionated phases and determine the preferred magnetic order. We discuss the similarities and differences of CCFO to RNiO_3 in the context of the Peierls and site-selective Mott scenarios.

II. COMPUTATIONAL METHOD

The LDA+ U calculations are performed using the augmented plane wave and local orbital (APW+lo) method implemented in the Wien2k package [51]. Following previous GGA+ U studies of CCFO [46, 47], the effective U values ($U_{\text{eff}} = U - J$) are chosen as $U_{\text{eff}} = 4.0$ eV and 7.0 eV for Fe and Cu ions, respectively. We have checked the robustness of the present result with respect to the

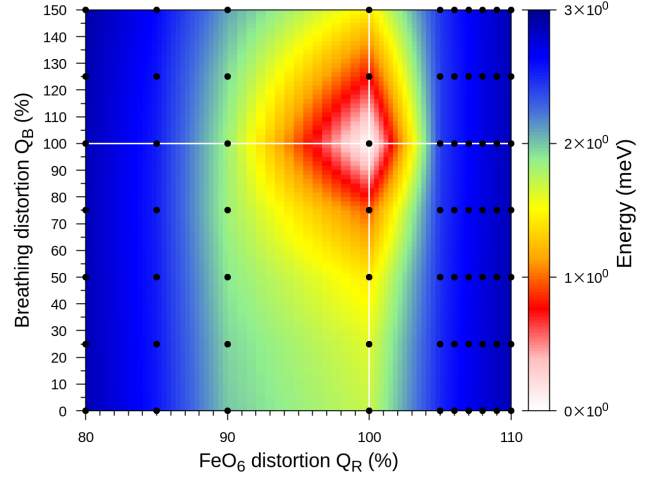


FIG. 2. Evolution of the LDA+ U total energy in the ferrimagnetic state with the breathing distortion Q_B and Q_R rotation mode. The energies are plotted in the logarithmic scale, see SM [45] for the energy cut for selected Q_R amplitudes. Note that 100% corresponds to the experimental amplitude.

choice of the exchange-correlation potential and U_{eff} parameters, see SM [45]. The reciprocal space cut-off K_{max} for the basis functions was chosen such that $R_{\text{MT}}K_{\text{max}} = 7.0$. The Brillouin zone was sampled with an $8 \times 8 \times 8$ mesh. To perform LDA+DMFT calculations [52–54], a tight-binding model spanning Cu $3d$, Fe $3d$ and O $2p$ bands, constructed using the wien2wannier [55] and wannier90 [56] codes, is augmented with the local Coulomb interaction on the Fe and Cu sites. We use the interaction parameters (in eV) $(U, J) = (7.50, 0.98)$ and $(6.80, 0.80)$ for the Cu and Fe $3d$ shells, respectively [57, 58]. To correct for the double counting of the Coulomb interaction, we shift the site energies of the Fe and Cu orbitals by the respective shell-averaged high-frequency limit (Hartree part) of the self-energy [58]. We show that our conclusions hold for a wide range of the double-counting corrections (treated as adjustable parameters), see SM [45]. In the DMFT self-consistent calculation, the continuous-time quantum Monte Carlo solver with density-density approximation to the on-site interaction was used to solve the auxiliary Anderson impurity model [59–62].

III. RESULTS

A. LDA+ U and Peierls mechanism

Since the LDA+ U approach cannot describe fluctuating local moments, we restrict ourselves to magnetically ordered phases (at $T = 0$). Overall, the FM solution has lower energy than antiferromagnetic or ferromagnetic solutions, except for $Q_R = 0\%$ where ferromagnetic alignment of all Fe and Cu moments is favored. Figure 2 shows the LDA+ U total energies for various amplitudes of the breathing Q_B and rotation Q_R distortions. For small Q_R

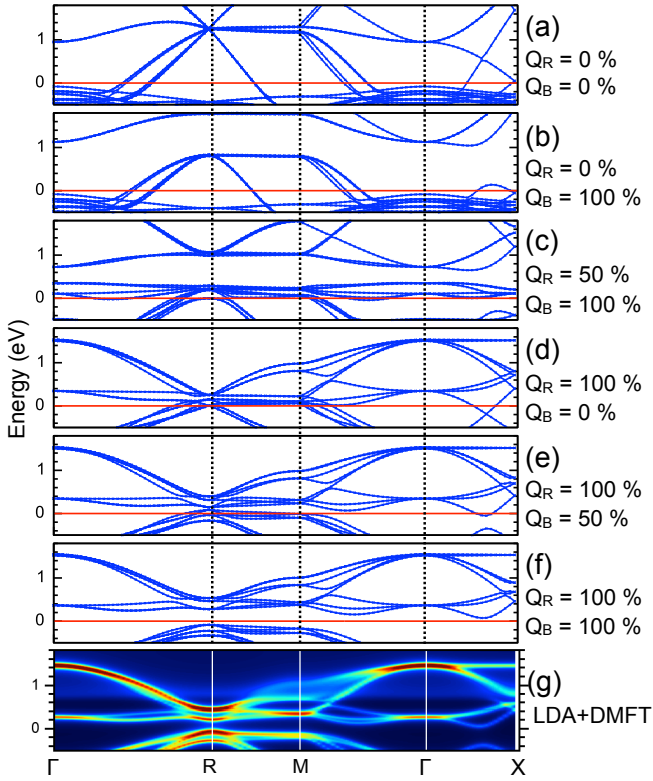


FIG. 3. (a-f) Low-energy bands for the majority spin channel calculated by LDA+ U for selected Q_R and Q_B amplitudes. The energy origin is taken at the Fermi energy (red line). (g) LDA+DMFT spectra in the ferrimagnetic solution (majority spin). The minority-spin bands can be found in SM [45].

the breathing distortion is unstable, while for larger Q_R a new local minimum appears at a finite Q_B amplitude. We find the global energy minimum close to the experimental Q_R and Q_B amplitudes (i.e. $Q_R = Q_B = 100\%$) irrespective of the interaction parameters within a realistic range [45].

In Figs. 3a-f we show the band structure in the vicinity of E_F at selected Q_R and Q_B . The depicted bands have dominantly majority-spin Fe $3d\ e_g$ character. The breathing distortion $Q_B=100\%$ opens a gap for all Q_R . However, only for $Q_R \gtrsim 75\%$ the Fermi level falls into the gap, allowing the system to gain electronic energy and thus stabilize the breathing distortion. The Q_R distortion reduces the e_g band width, which in turn pushes the band crossing ($Q_B=0$) at R -point to E_F , see Fig. 3. While at $Q_B=100\%$ the band crossing locates at the optimal position on the Fermi level, Fig. 3d, the insulating band structure is obtained already for $Q_B=75\%$. This picture is the Peierls-like instability for opening the gap, described in Refs. 28 and 34, in rare-earth nickelates.

The problem with this picture is that saturated spin polarization of the Fe e_g bands is necessary to open a gap at E_F [34], while experimentally the normal phase is paramagnetic. This criticism in CCFO is weaker than in case of the paramagnetic-metal to paramagnetic-

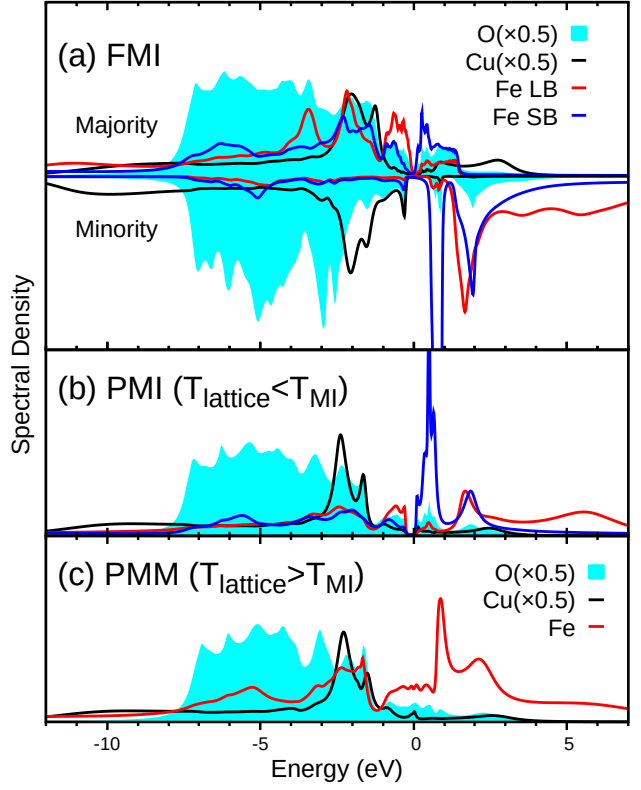


FIG. 4. The k -integrated LDA+DMFT spectra in (a) ferrimagnetic insulating (FMI), (b) paramagnetic insulating (PMI) and (c) paramagnetic metallic (PMM) solution. The two insulating solutions are obtained with the experimental low-temperature distorted structure (with Q_B), while the metallic one is obtained with the experimental high-temperature structure ($Im\bar{3}$).

insulator transition in $RNiO_3$ since short range magnetic order is expected above T_c in CCFO, where MIT and magnetic ordering take place simultaneously.

B. LDA+DMFT and site-selective Mott transition

The LDA+DMFT approach can capture the magnetically ordered phase as well as the paramagnetic state with fluctuating local moments. Our implementation of LDA+DMFT does not allow a reliable calculation of the free energy. Therefore we do not search for the most stable state as with LDA+ U , but only investigate the electronic structure above and below the experimental structural transition. In the following we analyze the ferrimagnetic and paramagnetic solutions. We find the ferrimagnetic solution to be stable for both distorted and undistorted structure up to 1200 K, which grossly overestimates the experimental T_c . We attribute it largely to the density-density approximation, in which the large Fe moments are treated as Ising rather than Heisenberg moments. The PM solutions are obtained by constraint

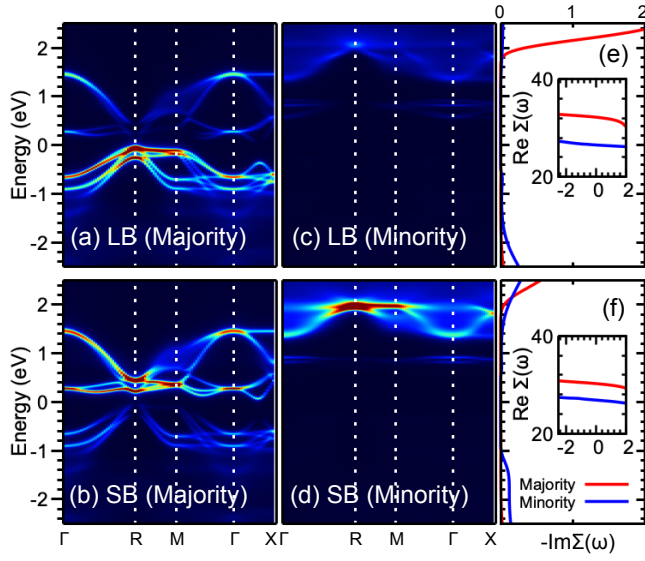


FIG. 5. LDA+DMFT valence spectra projected onto Fe $e_{g\sigma}$ -states on (a,c) long-bond (LB) and (b,d) short-bond (SB) site. The panels (a,b) and (c,d) are for the majority-spin and minority-spin channel in the ferrimagnetic solution, respectively. Total as well as Cu d -projected spectra can be found in SM. The imaginary part of the self-energies in the real-frequency domain for (e) LB and (f) SB site. The real part of the self-energies is shown in the inset.

for the DMFT self-energy of the Cu and Fe d electrons.

Figures 4ab show the k -integrated spectra of the ferrimagnetic and paramagnetic LDA+DMFT solutions for the experimental crystal structure. In agreement with experiment, we find a metallic solution in the undistorted structure (the FM solution not shown here is also metallic). The states around E_F have dominantly Fe e_g character. Unlike in RNiO_3 , we find a rather strong damping of the e_g states due to interaction with fluctuating t_{2g} moments (absent in RNiO_3). This explains smaller conductivity of metallic CCFO [42].

The LDA+DMFT solution in the distorted structure is insulating irrespective of the presence of the magnetic order. The FM state at the simulation temperature is fully saturated. The absence of spin fluctuations leads to a band structure that closely resembles the LDA+ U one, see Figs. 3fg. This is not surprising since the self-energy on both the SB and LB site, shown in Figs. 5ef, is dominated by the frequency-independent Hartree term with vanishing imaginary part around E_F . The gap then has a Peierls character between the LB-dominated valence and SB-dominated conduction band, Figs. 5ab, and the minority bands removed from the vicinity of E_F , Figs. 5cd.

The PM spectra in the distorted structure offer a rather different picture, Figs. 6abde. The Fe e_g bands are strongly damped and renormalized due to fluctuating t_{2g} moments. However, the main difference is the nature of the gap that is opened due to a pole in the LB self-energy, while the SB self-energy has a Fermi liquid character. The MIT in the PM phase thus has the

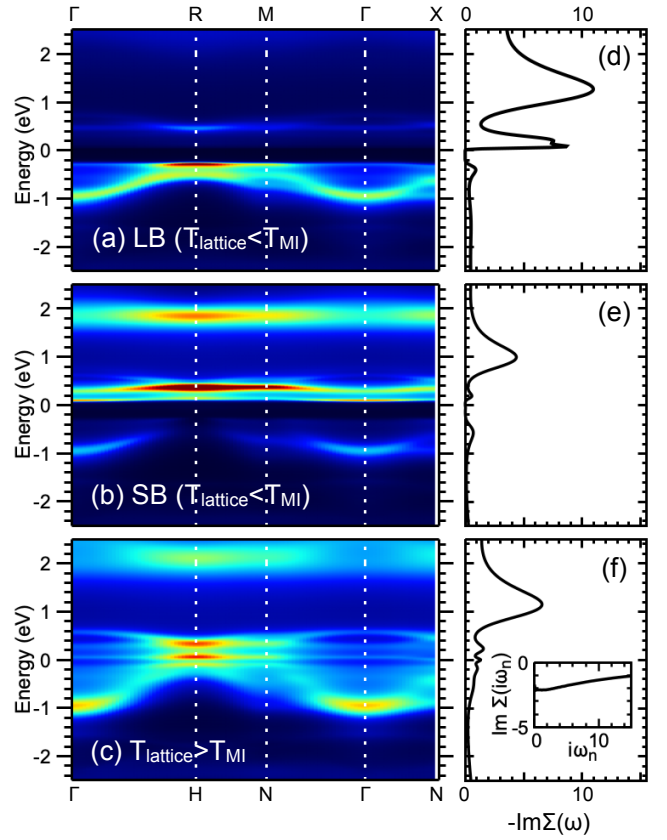


FIG. 6. LDA+DMFT valence spectra projected onto Fe $e_{g\sigma}$ -states on (a) long-bond (LB) and (b) short-bond (SB) site in the paramagnetic insulating solution obtained with the distorted structure (i.e. $Q_B = Q_R = 100\%$) (c) Fe $e_{g\sigma}$ -states in the paramagnetic metallic solution obtained with the experimental structure above the MI transition ($Im\bar{3}$). The imaginary part of the self-energies in the real-frequency domain is shown in panels (d-f). The inset in panel (f) shows the self-energy in the Matsubara-frequency domain.

site-selective Mott character [25, 37].

IV. DISCUSSION

We start our discussion by analysing the local physics on Fe sites in the site-selective Mott state. The LDA+DMFT calculation yields similar d -occupations (per site) of 5.18 and 5.08 on the LB and SB Fe sites, respectively. Although the charge fluctuation is slightly larger on the SB site, the local charge susceptibilities (charge-charge correlation function) on the two Fe sites, Figs. 7cd, resemble each other with almost incompressible Fe $3d$ states. The different nature of LB and SB sites is revealed by the local spin susceptibilities in Figs. 7ab, which yield the effective screened moments $m_{\text{scr}} = \sqrt{T\chi_{\text{loc}}}$ of 4.37 and 3.10 μ_B for the LB and SB sites, respectively. The long-lived moment on the SB site is in qualitative contrast with that in RNiO_3 with vanish-

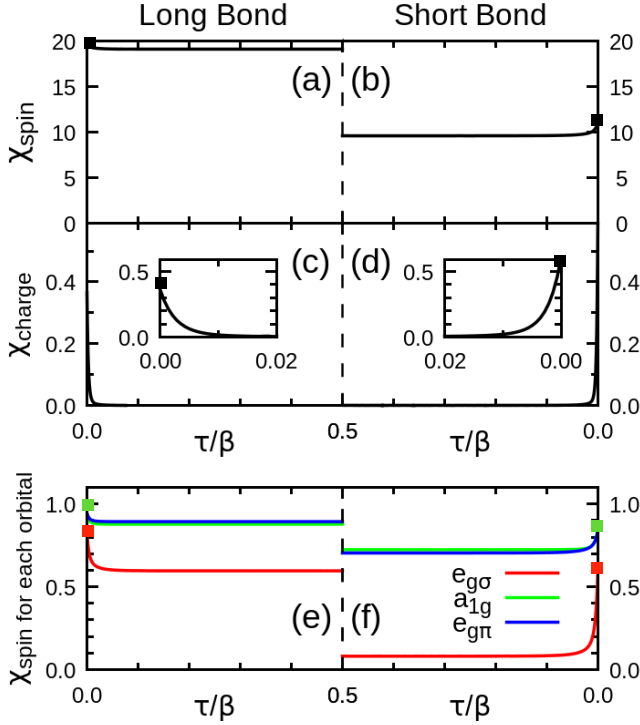


FIG. 7. Local spin/charge susceptibility in (a)/(c) long-bond and (b)/(d) short-bond Fe site calculated by LDA+DMFT. The orbital-diagonal contributions in the local spin susceptibility of (e) long-bond and (f) short-bond Fe site. Note that the rotation of the FeO_6 octahedra splits t_{2g} states into a_{1g} and doubly-degenerated $e_{g\pi}$ states. Square symbols in (e) and (d) mark the value at $\tau=0$.

ing m_{scr} on the SB Ni site [25, 32]. The orbital-diagonal contributions in the local spin susceptibility in Figs. 7e,f reveal that, while all d electrons contribute to the LB local moment, only the t_{2g} ones contribute on the SB site. This leads to the following site-disproportionation picture of CCFO: $2(d^5\bar{L}) \rightarrow t_{2g}^3[e_g^2\bar{L}_\sigma^2] (S=3/2) + t_{2g}^2e_g^2 (S=5/2)$, where \bar{L}_σ denotes a ligand hole that couples with the e_g states.

This picture is corroborated by the weights of atomic configurations (diagonal element of the site-reduced density matrix) in Fig. 8. The high-spin ($S=5/2$) state with $e_g^2t_{2g}^3$ configuration is dominant on the LB site. The SB Fe site shows a broader distribution of the atomic weights. This is to be attributed to the stronger covalent bonding with O sites. While this affects mostly the e_g orbitals, the abundance of the $e_g^1t_{2g}^4$ configuration shows that reducing the role of t_{2g} electrons to building of a rigid local moment is an approximation.

Next, we discuss the origin of the magnetic ordering. We find that both in the non-disproportionated metallic state and the disproportionated insulating state the Fe moment favor parallel (ferro- or ferrimagnetic) orientation. To understand this, we refer to the general picture of Zener double-exchange model [11] in which antiferromagnetically arranged local (t_{2g}) moments generate, via

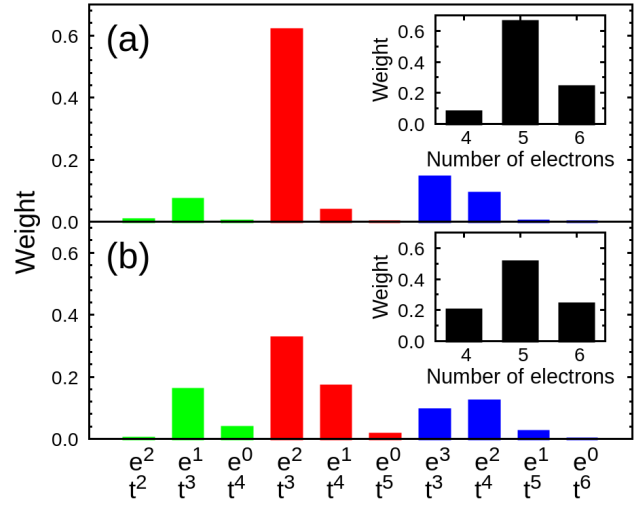


FIG. 8. Weights of dominant atomic states in $N=4$ (green), 5 (red) and 6 (blue) occupations on (a) long-bond and (b) short-bond Fe site. The atomic weights integrated in $N=4$, 5 and 6 sectors are shown in inset.

intra-atomic Hund's coupling, a staggered potential for the electrons in partially filled e_g bands. This increases the kinetic energy of the e_g electrons and thus favors FM alignment of the local moments. This mechanism, which is traditionally used to describe doped manganites, survives also in metallic systems with moderate fluctuations of t_{2g} charge [63] such as SrCoO_3 [64]. The metallic phase of CCFO is in this respect similar to the high-valence SrCoO_3 .

In the disproportionated state, the (staggered) antiferromagnetic potential leads to closing of the gap and thus insulator-compatible FM order is favored. The antiferromagnetic coupling of the Cu ($S=1/2$) and Fe moments observed in our calculations is not the glue of the ferromagnetic coupling of the Fe moments. A DMFT calculation with a paramagnetic constraint on the Cu site yields a ferrimagnetic insulating solution with almost unchanged Fe bands, see SM [45].

The key question concerning materials exhibiting a bond disproportionation such as RNiO_3 or the present CCFO is the site-selective Mott vs Peierls mechanism of the MIT. In the context of RNiO_3 , this question was addressed in a number of recent studies [25, 34, 37]. Due to the limitation of our present approach we are not able to provide a definite answer - magnetic ordering and site disproportionation take place simultaneously in CCFO. Nevertheless, the strikingly different band structures of FM and PM states in Fig. 5 and Fig. 6 open a question whether these are, in principle, compatible with each other, i.e., can one go from the PM band structure to the FM one without closing the gap? The gap in the PM state relies on the pole in the self-energy of the LB site, while in the FM state the Hartree (energy independent) shift of the spin-minority band above the chemical potential is crucial.

To understand how the PM Mott state can evolve in the FM one without closing the gap, we invoke a toy model of Ref. 37 that captures essentials of the site-disproportionated Mott state and the behavior of the self-energy pole when going from PM to spin-polarized Mott insulator. The authors of Ref. 65 showed that the magnetic ordering (in one-band Hubbard model) introduces, in addition to the spin-dependent Hartree contribution to the self-energy, a spin dependent shift of the self-energy along the frequencies. This way the LB and SB site self-energies evolve from the PM state, Figs. 6de, to the FM state, Figs. 5ef. Introducing this behavior by hand to the toy model, one can go smoothly from the PM to the FM state without moving the gap away from the E_F as demonstrated by a movie in SM [45].

V. CONCLUSION

By means of LDA+ U and LDA+DMFT methods, we investigated insulating and magnetic properties in $\text{CaCu}_3\text{Fe}_4\text{O}_{12}$, consisting of high Fe^{4+} valence. By a systematic LDA+ U calculation combined with a distortion-mode analysis, we revealed an underlying Peierls instability to open the electronic gap in the ferrimagnetic ordered phase. The LDA+DMFT simulation indicates that the site-selective Mott mechanism also opens the insulat-

ing gap in the experimental distorted structure. In the site-disproportionated state of $\text{CaCu}_3\text{Fe}_4\text{O}_{12}$, the two e_g electrons on the short-bond Fe site couples with oxygen p holes, forming a singlet, while t_{2g} moments are robust in both long- and short-bond Fe sites, leading to the site-disproportionation picture: $2(d^5\bar{L}) \rightarrow t_{2g}^3[e_g^2\bar{L}_\sigma^2]$ ($S = 3/2$) + $t_{2g}^3e_g^2$ ($S = 5/2$). In contrast to rare-earth nickelates RNiO_3 , the paramagnetic site-selective Mott phase is not observed experimentally. The active Fe t_{2g} moment ($S = 3/2$), absent in RNiO_3 , stabilizes the ferrimagnetic order via the double-exchange mechanism. We discussed the spectral change from the site-selective Mott to ferrimagnetic Peierls-like insulator.

ACKNOWLEDGMENTS

We thank A. Georges, I. Yamada, M. Mizumaki, Y. Uchimura, J. Fernández Afonso and A. Sotnikov for fruitful discussions. A.H, M.W, and J.K were supported by the European Research Council (ERC) under the European Union's Horizon 2020 research and innovation programme (Grant Agreement No. 646807-EXMAG). A.H. was supported by JSPS KAKENHI with Grant Numbers 23K03324 and 23H03817. The computational calculations were performed at the Vienna Scientific Cluster (VSC).

-
- [1] M. Imada, A. Fujimori, and Y. Tokura, *Rev. Mod. Phys.* **70**, 1039 (1998).
 - [2] D. I. Khomskii, *Transition Metal Compounds* (Cambridge University Press, Cambridge, England, 2014).
 - [3] Y. Tanabe and S. Sugano, *J. Phys. Soc. Jpn.* **9**, 753 (1954).
 - [4] P. Werner and A. J. Millis, *Phys. Rev. Lett.* **99**, 126405 (2007).
 - [5] A. G. Gavriliuk, V. V. Struzhkin, I. S. Lyubutin, S. G. Ovchinnikov, M. Y. Hu, and P. Chow, *Phys. Rev. B* **77**, 155112 (2008).
 - [6] J. Kuneš and V. Křápek, *Phys. Rev. Lett.* **106**, 256401 (2011).
 - [7] J. F. Afonso, A. Sotnikov, A. Hariki, and J. Kuneš, *Phys. Rev. B* **99**, 205118 (2019).
 - [8] G. Khaliullin, *Phys. Rev. Lett.* **111**, 197201 (2013).
 - [9] J. Kuneš and P. Augustinský, *Phys. Rev. B* **90**, 235112 (2014).
 - [10] T. Yamaguchi, K. Sugimoto, and Y. Ohta, *J. Phys. Soc. Jpn.* **86**, 043701 (2017).
 - [11] C. Zener, *Phys. Rev.* **82**, 403 (1951).
 - [12] Y. Tokura and Y. Tomioka, *J. Magn. Magn. Mater.* **200**, 1 (1999).
 - [13] J. van den Brink, G. Khaliullin, and D. Khomskii, *Phys. Rev. Lett.* **83**, 5118 (1999).
 - [14] K. I. Kugel and D. I. Khomskii, *Phys.-Uspekhi* **25**, 231 (1982).
 - [15] A. M. Glazer, *Acta Crystallogr. B* **28**, 3384 (1972).
 - [16] P. M. Woodward, *Acta Crystallogr. B* **53**, 32 (1997).
 - [17] C. J. Howard and H. T. Stokes, *Acta Crystallogr. B* **54**, 782 (1998).
 - [18] H. A. Jahn, E. Teller, and F. G. Donnan, *Proceedings of the Royal Society of London. Series A - Mathematical and Physical Sciences* **161**, 220 (1937).
 - [19] J. B. Goodenough, *Annu. Rev. Mater. Sci.* **28**, 1 (1998).
 - [20] I. B. Bersuker, *The Jahn-Teller Effect* (Cambridge University Press, Cambridge, England, 2014).
 - [21] J. Kanamori, *J. Appl. Phys.* **31**, S14 (1960).
 - [22] I. I. Mazin, D. I. Khomskii, R. Lengsdorf, J. A. Alonso, W. G. Marshall, R. M. Ibberson, A. Podlesnyak, M. J. Martínez-Lope, and M. M. Abd-Elmeguid, *Phys. Rev. Lett.* **98**, 176406 (2007).
 - [23] Y. Tokura and N. Nagaosa, *Science* **288**, 462 (2000).
 - [24] E. Pavarini and E. Koch, *Phys. Rev. Lett.* **104**, 086402 (2010).
 - [25] H. Park, A. J. Millis, and C. A. Marianetti, *Phys. Rev. Lett.* **109**, 156402 (2012).
 - [26] E. Greenberg, I. Leonov, S. Layek, Z. Konopkova, M. P. Pasternak, L. Dubrovinsky, R. Jeanloz, I. A. Abrikosov, and G. K. Rozenberg, *Phys. Rev. X* **8**, 031059 (2018).
 - [27] A. Hariki, K.-H. Ahn, and J. Kuneš, *Phys. Rev. B* **104**, 235101 (2021).
 - [28] S. Lee, R. Chen, and L. Balents, *Phys. Rev. Lett.* **106**, 016405 (2011).
 - [29] B. Lau and A. J. Millis, *Phys. Rev. Lett.* **110**, 126404 (2013).
 - [30] S. Johnston, A. Mukherjee, I. Elfimov, M. Berciu, and G. A. Sawatzky, *Phys. Rev. Lett.* **112**, 106404 (2014).

- [31] R. Jaramillo, S. D. Ha, D. M. Silevitch, and S. Ramathan, *Nat. Phys.* **10**, 304 EP (2014).
- [32] A. Subedi, O. E. Peil, and A. Georges, *Phys. Rev. B* **91**, 075128 (2015).
- [33] V. Bisogni, S. Catalano, R. J. Green, M. Gibert, R. Scherwitzl, Y. Huang, V. N. Strocov, P. Zubko, S. Balandeh, J.-M. Triscone, G. Sawatzky, and T. Schmitt, *Nat. Commun.* **7**, 13017 (2016).
- [34] A. Mercy, J. Bieder, J. Íñiguez, and P. Ghosez, *Nat. Commun.* **8**, 1677 (2017).
- [35] J. Varignon, M. N. Grisolia, J. Íñiguez, A. Barthélémy, and M. Bibes, *npj Quantum Materials* **2**, 21 (2017).
- [36] P. Seth, O. E. Peil, L. Pourvorskii, M. Betzinger, C. Friedrich, O. Parcollet, S. Biermann, F. Aryasetiawan, and A. Georges, *Phys. Rev. B* **96**, 205139 (2017).
- [37] J. Ruppen, J. Teyssier, O. E. Peil, S. Catalano, M. Gibert, J. Mravlje, J.-M. Triscone, A. Georges, and D. van der Marel, *Phys. Rev. B* **92**, 155145 (2015).
- [38] Y. Shimakawa, *Inorg. Chem.* **47**, 8562 (2008).
- [39] J.-G. Cheng, J.-S. Zhou, Y.-F. Yang, H. D. Zhou, K. Matsumabayashi, Y. Uwatoko, A. MacDonald, and J. B. Goodenough, *Phys. Rev. Lett.* **111**, 176403 (2013).
- [40] Y. W. Long, N. Hayashi, T. Saito, M. Azuma, S. Muranaka, and Y. Shimakawa, *Nature* **458**, 60 EP (2009).
- [41] D. Meyers, S. Mukherjee, J. G. Cheng, S. Middey, J. S. Zhou, J. B. Goodenough, B. A. Gray, J. W. Freeland, T. Saha-Dasgupta, and J. Chakhalian, *Sci. Rep.* **3**, 1834 (2013).
- [42] Y. Shimakawa, *J. Phys. D: Appl. Phys.* **48**, 504006 (2015).
- [43] I. Yamada, M. Ochi, M. Mizumaki, A. Hariki, T. Uozumi, R. Takahashi, and T. Irifune, *Inorg. Chem.* **53**, 7089 (2014).
- [44] I. Yamada, K. Takata, N. Hayashi, S. Shinohara, M. Azuma, S. Mori, S. Muranaka, Y. Shimakawa, and M. Takano, *Angew. Chem. Int. Ed.* **47**, 7032 (2008).
- [45] See Supplementary Material for details of computations and structural-mode analysis, which includes Ref. [48, 66].
- [46] X. Hao, Y. Xu, F. Gao, D. Zhou, and J. Meng, *Phys. Rev. B* **79**, 113101 (2009).
- [47] T. Ueda, M. Kodera, K. Yamauchi, and T. Oguchi, *J. Phys. Soc. Jpn.* **82**, 094718 (2013).
- [48] M. Mizumaki, W. T. Chen, T. Saito, I. Yamada, J. P. Attfield, and Y. Shimakawa, *Phys. Rev. B* **84**, 094418 (2011).
- [49] K. Momma and F. Izumi, *J. Appl. Crystall.* **44**, 1272 (2011).
- [50] J. M. Perez-Mato, D. Orobengoa, and M. I. Aroyo, *Acta Crystallogr. A* **66**, 558 (2010).
- [51] P. Blaha, K. Schwarz, G. Madsen, D. Kvasnicka, and J. Luitz, *WIEN2k, An Augmented Plane Wave + Local Orbitals Program for Calculating Crystal Properties* (Karlheinz Schwarz, Techn. Universitat Wien, Austria, 2001, ISBN 3-9501031-1-2).
- [52] G. Kotliar, S. Y. Savrasov, K. Haule, V. S. Oudovenko, O. Parcollet, and C. A. Marianetti, *Rev. Mod. Phys.* **78**, 865 (2006).
- [53] J. Kuneš, I. Leonov, M. Kollar, K. Byczuk, V. I. Anisimov, and D. Vollhardt, *Eur. Phys. J. Spec. Top.* **180**, 5 (2009).
- [54] A. Georges, G. Kotliar, W. Krauth, and M. J. Rozenberg, *Rev. Mod. Phys.* **68**, 13 (1996).
- [55] J. Kuneš, R. Arita, P. Wissgott, A. Toschi, H. Ikeda, and K. Held, *Comput. Phys. Commun.* **181**, 1888 (2010).
- [56] A. A. Mostofi, J. R. Yates, G. Pizzi, Y.-S. Lee, I. Souza, D. Vanderbilt, and N. Marzari, *Comput. Phys. Commun.* **185**, 2309 (2014).
- [57] V. I. Anisimov, J. Zaanen, and O. K. Andersen, *Phys. Rev. B* **44**, 943 (1991).
- [58] J. Kuneš, D. M. Korotin, M. A. Korotin, V. I. Anisimov, and P. Werner, *Phys. Rev. Lett.* **102**, 146402 (2009).
- [59] P. Werner, A. Comanac, L. de' Medici, M. Troyer, and A. J. Millis, *Phys. Rev. Lett.* **97**, 076405 (2006).
- [60] L. Boehnke, H. Hafermann, M. Ferrero, F. Lechermann, and O. Parcollet, *Phys. Rev. B* **84**, 075145 (2011).
- [61] H. Hafermann, K. R. Patton, and P. Werner, *Phys. Rev. B* **85**, 205106 (2012).
- [62] A. Hariki, A. Yamanaka, and T. Uozumi, *J. Phys. Soc. Jpn.* **84**, 073706 (2015).
- [63] A. Sotnikov, A. Cichy, and J. Kuneš, *Phys. Rev. B* **97**, 235157 (2018).
- [64] J. Kuneš, V. Křápek, N. Parragh, G. Sangiovanni, A. Toschi, and A. V. Kozhevnikov, *Phys. Rev. Lett.* **109**, 117206 (2012).
- [65] G. Sangiovanni, A. Toschi, E. Koch, K. Held, M. Capone, C. Castellani, O. Gunnarsson, S.-K. Mo, J. W. Allen, H.-D. Kim, A. Sekiyama, A. Yamasaki, S. Suga, and P. Metcalf, *Phys. Rev. B* **73**, 205121 (2006).
- [66] J. P. Perdew, K. Burke, and M. Ernzerhof, *Phys. Rev. Lett.* **77**, 3865 (1996).